The Asian Review of Civil Engineering
ISSN: 2249-6203 (P) Vol.1 No.2, 2012, pp.36-46

DOI: https://doi.org/10.51983/tarce-2012.1.2.2184

Finite Element Analysis for Machinability Test of Laser Sintered Material

Ahmad Shahir bin Jamaludin, Abdullah bin Yassin and Mohd. Shahril bin Osman

Department of Mechanical and Manufacturing Engineering,

Faculty of Engineering, Universiti Malaysia Sarawak - 94300, Kota Samarahan, Sarawak

E-mail: aero_zephyr@yahoo.com

(Received on 25 August 2012 and accepted on 25 November 2012)

Abstract **- In this paper, finite element analysis (FEA) on machinability of laser sintered material with mean of predicted cutting force and temperature distribution is explained. The process involved 2D orthogonal down-cut milling with the application of two dimension thermo mechanical plane strain model. The updated Lagrangian formulation was used where cutting simulation does not involve element separation but remesh automatically when element distorted critically. AISI1055 mild steel properties were used as the comparison. Various types of friction models were adopted in obtaining precise results. Predicted cutting force and cutting edge temperature are validated against corresponding experimental values by previous researchers. From the simulations, the shear friction model of 0.8 is the best friction model where 10% errors were obtained for comparison mild steel AISI1055 FEA results with the experimental approach for increasing radial depth. Lower cutting force predicted for laser sintered materials compared to AISI1055 due to lower Young modulus. Cutting edge temperature predicted for laser sintered material is higher due to its low thermal conductivity compared to AISI1055.**

Keywords: **Finite element method (FEM), 2D Orthogonal end milling, Cutting force prediction, Cutting temperature prediction, Friction model**

I. Introduction

Injection moulding is one of the most versatile and important operations for mass production of complex plastic parts with excellent dimensional tolerance. In the conventional mould manufacturing, subtractive processes such as high speed machining (HSM) [1] and electro discharge machining (EDM) are applied to make the mould from hardened steel [2]. This conventional mould manufacturing is not economic because these subtractive processes are time consuming. Production time is one of the key factors for success in the consumer product marketplace. Various negative effects such as chatter, wobble and impact loading cause by the deflection at the cutting edge in making a precise mould having a deep rib could result in poor dimensional accuracy. Easiest way to control the tool deflection is by reducing the tool length. Therefore, this conventional mould manufacturing is unsuitable in making a complicated injection mould.

Stereolithography (SL) application has reduced mould manufacturing's production time and cost [3]. Furthermore, a mould having a deep rib can be created. However, due to its low flexural stresses, life span of the mould produce from SL is short [3]. Introducing Selective Laser Sintering (SLS) where the application of a laser beam to irradiate metal powder in making three dimensional shaped parts could greatly reduce mould manufacturing time and increase its life span. Nevertheless, resulting part offers limited dimensional accuracy and poor surface roughness [4].

Milling-combined laser sintering system (MLSS) that combines laser sintering of fine metallic powder and high speed milling has been developed to overcome these deficiencies. Small ball end mill is employed to machine complicated mould features because the ball end mill capable in machining free-form surfaces [5]. Therefore, making complicated mould having a deep rib is feasible and the dimensional accuracy is also improved.

In MLSS, about 30% from the total production time in making a mould is required for high speed machining (HSM). It is crucial to understand the machinability of the laser-sintered material where cutting the laser-sintered material efficiently is one of the important factors in gaining maximum economic benefit from MLSS.

According to S. Kalpakjian [4], machinability of workpiece materials refers to the less difficulty with which a given metal can be machined to an adequate surface finish. Materials with good achievability require less cutting force, low processing time, obtainable better surface finish, and cause low gradual failure on cutting tool.

Surprisingly, machinability study of laser-sintered material did not attract much attention from the researchers

[6]. According to experimental studied that been done by A.Yassin *et al.,* laser sintered material can be considered as hard to machine, due to its low thermal conductivity, and high material hardness. Since laser sintered material is powder metallurgical base material, its porosity makes it hard to obtain acceptable surface roughness, although low cutting force needed to cut the materials [6]. Therefore, if we want to take advantage of MLSS as a new invention in mould making, there will be a need to study machinability of laser sintered material.

In this study, machinability of laser-sintered material was analyzed with mean of cutting force and cutting temperature generated on the cutting tool during the machining process by FE simulation. In addition, comparison with the machining processes by FE simulation for mild steel; AISI1055 was also been done.

A. Finite Element Analysis (FEA)/Finite Element Method (FEM)

Finite element analysis (FEA) or also called finite element method (FEM) is a numerical technique breaking up a problem into small regions called elements in solving a simulation model. Finite element method (FEM) has become distinguished in simulating high speed machining and convenient in saving cost, time, and capable to forecast effects of cutting parameter on cutting force, cutting edge temperature and chip formations[7,8]. With the application of FEM, cutting forces and temperatures obtained can be used in estimating the optimum cutting conditions such as cutting speed, cutting depth, etc.

One of the most simplified models of FEA for machining is orthogonal cutting. Orthogonal cutting involved cutting edge moves perpendicular to the relative motion between cutting tool and workpiece to remove unwanted material from the workpiece with constant uncut chip thickness [7]. In milling processes, uncut chip thickness vary depends on fix parameters of radial depth, cutting tool diameter and cutting feed and cutting edge radial position [8].

The earlier researchers developed 2D orthogonal cutting such as Usui and Shirakashi obtained steady state cutting using iterative convergence method in FEM [9]. Strenkowski and Carroll developed numerical model without a preformed chip using updated Lagrangian code [10]. Recent 2D model developed by L. Filice *et al.* [7] and T. Özel [8], applied friction condition in obtaining more practical data. J.P. Davim et al. studied plastic strain and plastic strain rate in machining AISI1045 FEM simulation [11]. Updated Lagrangian formulation on 2D thermo mechanical plane strain FEM model will be applied in the investigation.

Widely known materials such as mild steel AISI1045 [11], aluminium (Al7075) [12], titanium alloy (Ti6Al-4V) [13] and AISI P20 mould steel alloy [14] was done in FEM machining simulation and have a quite good concurrency with experimental results. In this study, laser sintered material will be applied as main material properties and AISI1055 will be the comparison. A. Yassin and T. Furumoto et al. studied the machinability of laser-sintered materials [6,15,16] experimentally without FEM analysis. Therefore, application of FEM could extend the knowledge of MLSS and laser sintered material.

In this study, finite element models of the end milling process were done in 2D orthogonal cutting. In addition, results obtained from FEM simulation will be compared with the previous experimental results were done by A. Yassin *et al.* in 2009 [6].

II. Finite Element Model

During the experimental study by A. Yassin, two flute ball end mill were used [6]. The tool geometry was then being developed into 2D orthogonal finite-element model as shown in Figure 1. This 2D FEM model is based on previous FEM machining models that been developed by L. Filice et al. and T. Özel [7, 8]. The model was developed only for a small part of the tool where the main contact between tool and workpiece occur. Tool edge radius, r equal to 10μm was used according to the original cutting tools [6]. This could define more realistic simulation to designate the experimental approach by A. Yassin *et al.* [6]. Table I show the summarization of the cutting tool characteristic in this study.

In 2D analysis, complicated ball part of the end mill was simplified where the maximum effective radius, R_{ef} was considered as the cutting tool rotation radius in obtaining estimated cutting force and estimated cutting temperature. The size of rotation radius depends on the type of ball end milling procedure during the experiment. Figure 2 shows the diagram of the peripheral milling process.

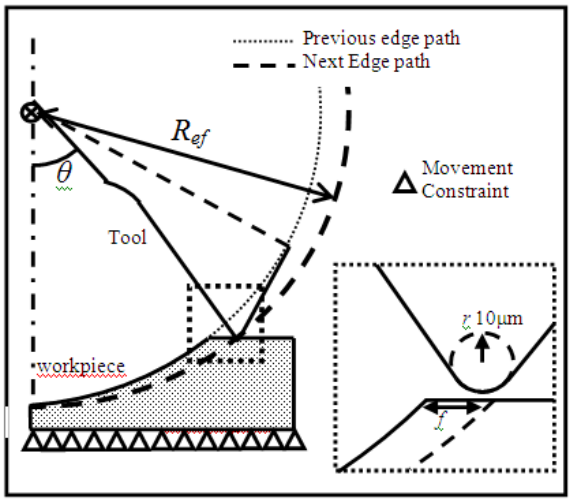

TABLE I CUTTING TOOL GEOMETRY

Tool diameter, D [mm]	6.0
Tool maximum effective radius of revolution, R_{ef} [mm]	3.0
Tool rake angle, α [°]	5.0
Tool clearance angle, γ [°]	12.0
Tool edge radius, r [mm]	0.01
Feed rate, f [mm/tooth]	0.01

Fig. 1 Simplified Tool And Workpiece Fem Model

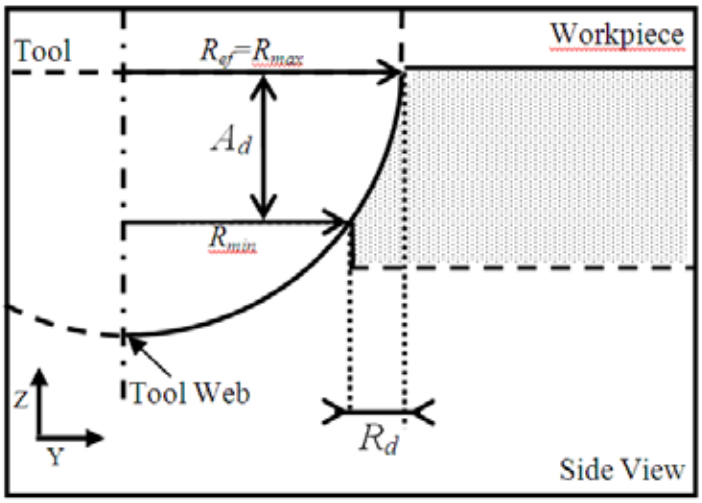

Fig. 2 Peripheral milling on side view

In this study, the tool geometry was adjusted to the experimental approach of peripheral milling by A. Yassin *et al.* [6]. Peripheral milling is the process where teeth located on the periphery of the cutter body generates the milled surface.

A. FE model Meshing

Isoparametic quadrilaterals mesh and adapted remeshing technique were used to mesh the 2D FE model. Isoparametic quadrilaterals mesh provides fewer element requirements and capable to rotate arbitrarily [17]. Adapted remeshing technique capable to remesh the model if critical element distortion existed during the simulation and this technique does not need element separation [7, 8]. Commercially available FE software that capable to execute both isoparametic quadrilaterals meshing and adapted remeshing technique was applied.

Denser and fine meshes were only applied at the tool edge – workpiece contact area where main mechanical work and large elastic-plastic deformation were generated. This meshing technique will ensure lighter and precise simulations can be done for the study. 2000 elements were use for workpiece, and 1000 elements were use for cutting tool mesh. Figure 3 shows an example of isoparametic quadrilaterals mesh with mesh density control that was applied in this study.

The cutting processes were assumed as ideal without cutters run-out (rigid). Workpiece will experience elastic-plastic deformation when tool - workpiece contact existed [7, 8].

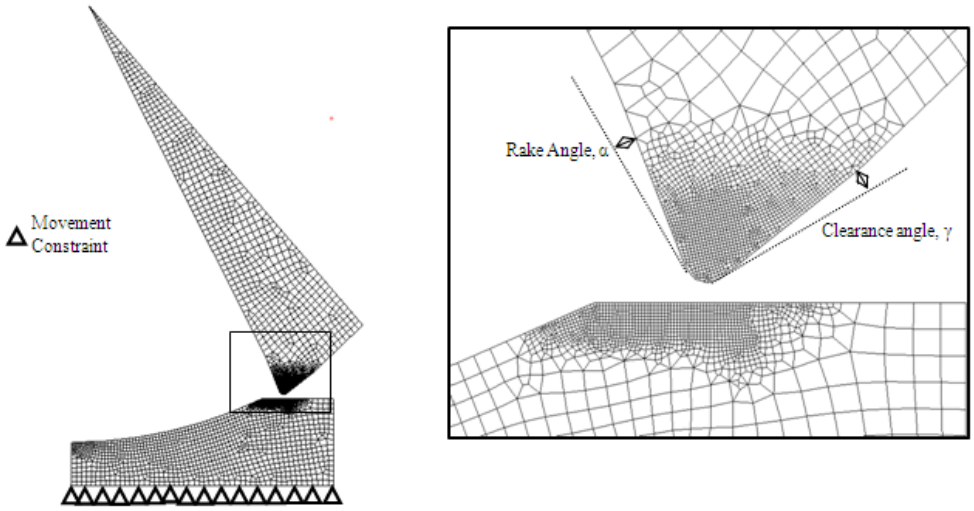

Fig. 3 Model meshing and density

B. Contact Length

Kato *et al.* [18] contact length model were use as tool-workpiece contact length in the simulation as shown in Eq. 1.

$$L_c = 2h \tag{1}$$

L_c is tool-workpiece contact length and h in the undeformed chip thickness

C. Friction Models

Frictional stress on rake face of tool is assumed constant and low stress variation of frictional stress, τ and normal stress, σ_n are neglected [8]. This can be expressed with following Eq. 2.

$$\tau = mk \tag{2}$$

m is friction factor from 0.6 to 0.9 and k is shear flow stress of the work material.

D. Heat Generation

In this study, all the mechanical work done in the machining process is assumed fully converted into heat [19]. Heat generation Q_r (W) in the primary deformation zone is equal to the rate of energy consumption during metal cutting and shown by Eq. 3.

$$Q_r = W_c = F_v V \tag{3}$$

F_v (N) is the cutting force and V (m/sec) is the cutting speed. Heat generation due to metal cutting was divided between tool, workpiece and chip. Heat flux, q (W/mm^2) may be calculated from the heat generation and contact area obtained from the simulation as Eq. 4 [20].

$$q = Q_r / L_c b \tag{4}$$

L_c (mm) and b (mm) are contact length and cutting width.

E. Thermal Boundaries

Thermal boundary conditions are important in determining temperature gradient in metal cutting. In Figure 3, C'-C" defined the tool-chip contact length, L_c where contact between the tool and the workpiece is assumed thermally perfect and a large value of h=1000 (kW/m^{2}K) is employed according to N.A. Abukhshim *et al.* [21].

Heat loss of the tool and workpiece at free surface to the environment is defined to be caused by convection where heat convection coefficient of 20 (W/m^{2}K) is employed to C"-A, D-E, H-D and B-C' according to L. Filice *et al.* [7].

The boundaries that are sufficiently far apart from the cutting zone is assumed to be not affected in temperature and thus, boundaries A-B, E-F and F-G are fixed with environment temperature, 20 (^{o}C) according to N.A. Abukhshim *et al.* [21]. Heat loss due to radiation is neglected.

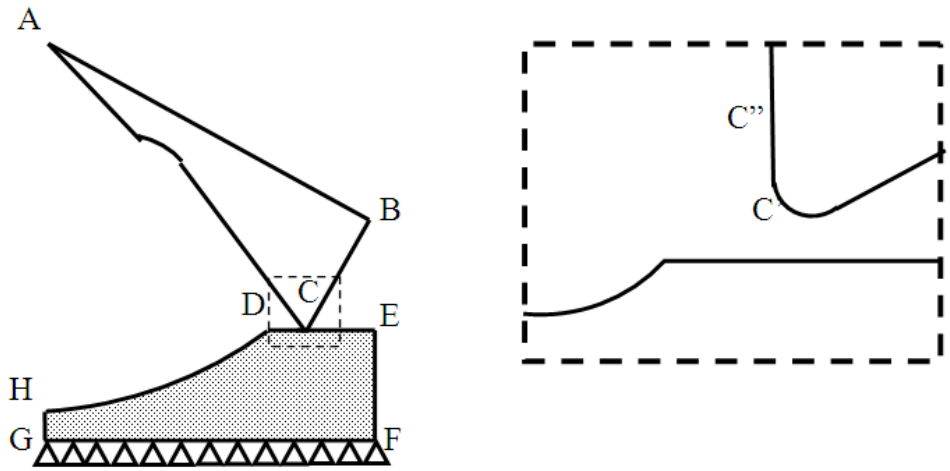

Fig. 4 Thermal boundaries on tool and workpiece

F. Data Collections

Figure 5 shows the schematic diagram of cutting tool and optical fiber position where cutting temperature values were taken from the simulation and measured during the experiment by A. Yassin *et al.* [6].

In comparing the predicted cutting edge temperature with the experimental results, air cutting time and cooling effect have to be taken into consideration. According to A. Hosokawa *et al.*, the temperature at a given time after the tool finishes cutting the workpiece and revolves is given by Eq. 5.

$$T_{\psi}(\delta)=(T_r-T_0)e^{-a\delta}+T_r \quad (5)$$

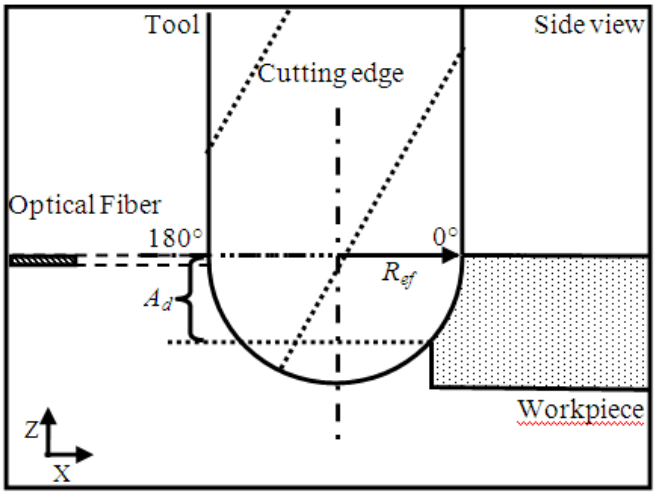

Fig. 5 Temperature Measurement Schematic

T_{ψ} (°C) is the temperature at a given air cutting time, T_r (°C) is the instantaneous cutting temperature after tool finishes cutting the workpiece, δ (s) is the air cutting time, T_0 is the room temperature and a=0.3 is cooling constant which is determined from A. Hosokawa *et al.* [22].

G .Cutting Conditions and Materials Properties

Table II shows characteristic morphology of metallic powder, before it was sintered with medium energy density, 9.0 (J/mm^2) to form laser sintered material, LSMeρ9. According to A. Yassin *et al.*, hardness and density of laser sintered material show increasing value when sintered with low energy density, 2.0 (J/mm^2) to medium energy density, 9.0 (J/mm^2). The values were increase from 211 ($HV_{0.3}$) to 275 ($HV_{0.3}$) for material hardness and 6950 (kgm^{-3}) to 7680 (kgm^{-3}) for material density. However, almost equal value of material hardness, 270 ($HV_{0.3}$) and density 7680 (kgm^3) obtained when the metallic powder was sintered with high-energy density, 20 (J/mm^2). The laser sintered material properties were taken for the inner work material surface where metallic powder is fully melted due to heat and reheat processes which is 1.0 [mm] from the periphery surface[6]. Materials properties and cutting conditions are shown in Tables III and 4 [16,17].

TABLE II PROPERTIES OF METALLIC POWDER

Materials	SCM	Ni	Cu
Powder Density (kg/m^3)	4690	4040	4690
Specific Heat (J/kgK)	450	490	380
Thermal Conductivity (W/mK)	0.13	0.17	0.17
Particle Diameter (μm) 3	0	30	30
Percent of Composition (%)	70 2	0	10

SCM : Chrome Molybdenum Steel

TABLE III TOOL AND WORKPIECE MATERIAL PROPERTIES

Materials	WC (Tool)	LSMEρ9	AISI1055
Young Modulus, E (GPa)	650	124	250
Poisson Ratio, ε	0.25	0.3	0.3
Thermal Conductivity, k (W/mK)	15	10	53
Density, ρ (kg/m^3)	14900	7680	7850
Specific Heat, c (J/kgK)	334	450	486
Hardness Vickers, $HV_{0.3}$	1400	275	145

TABLE IV CUTTING CONDITIONS

Cutting tool diameter, D (mm)	0.6,1.0,2.0,6.0
Radial depth of cut, R_d (mm)	0.1-0.6
Revolution Speed (RPM)	4000-40000
Cutting speed, V_c (m/min)	75-754
Cutting feed, f (mm/tooth)	0.01

H. FEM Results Validation

Estimated cutting force and cutting edge temperature by the study's FE analyses are validated against corresponding experimental values by A. Yassin *et al.* [6].

III. RESULTS AND DISCUSSION

A. *Cutting Forces Analysis*

Figure 6 shows cutting force profile obtained from the simulation. Similar values obtained from the simulation due to the rigid tool assumption during the simulation. A single value was taken as the cutting force for the analysis. Figure 7 shows the comparison of different shear friction models and different radial depths for AISI1055 at cutting speed 75 m/min.

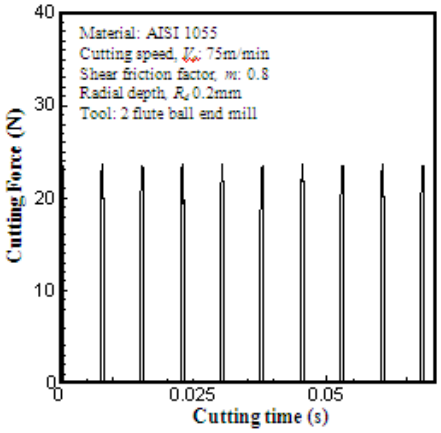

Fig. 6 Cutting force profile

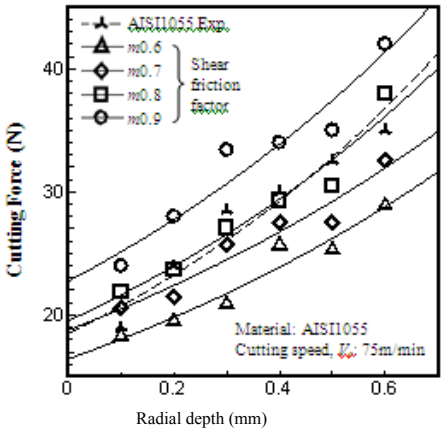

Fig. 7 Effect of frictions model and radial depth on cutting force

From Figure 7, shear friction factor, m and radial depth, R_d shows direct proportional effect on cutting force. This is due to increasing frictional stress on the rake face and chip removal rate (mm^3/s) during metal cutting. Shear friction factor 0.8 can be considered as the best shear friction model in estimating cutting force. This is due to lowest errors (10%) shown and with this shear friction model, high precision simulation results that related to cutting force such as cutting temperature could be obtained.

Figure 8 shows the cutting force comparison between simulation and experimental results for AISI1055 and LSMEρ9. The cutting processes were simulated by FEM with the same shear friction model of m0.8 and cutting speed 75m/min for both materials. Cutting force of AISI1055 is higher than LSMEρ9 at the same cutting rotational speed. This is because of LSMEρ9 is easy to deform due to lower Young Modulus (124GPa) than AISI1055 (250GPa).

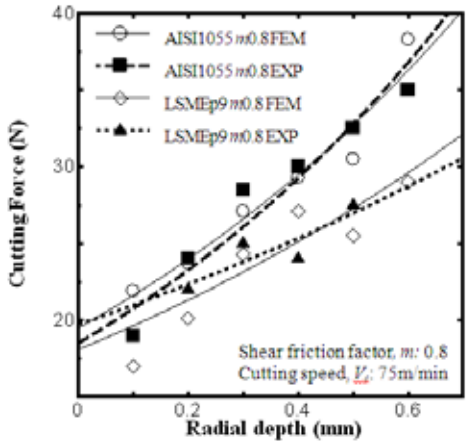

Fig. 8 Effect of Young modulus and radial depth on cutting force

B. Cutting Temperature Analysis

Figure 9 shows the temperature profile for machining LSMEρ9 at cutting speed 754m/min and 0.1mm radial depth at 0° (Figure 5). A single maximum value was taken as maximum cutting temperature. After considering the cooling effect during ball end milling processes base on Eq.5, comparisons of estimated cutting temperature of AISI1055 and LSMEρ9 with experimental results are shown in Figure10.

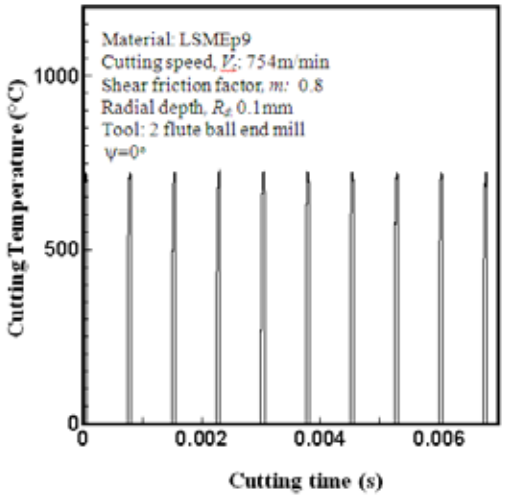

Fig. 9 Cutting temperature profile

FEM simulation of LSMEρ9 shows cutting edge temperature error below 5% compared to the experimental results. From Figure 10, it is known that LSMEρ9 shows higher temperature gradient than AISI1055. This is due to the lower thermal conductivity of LSMEρ9 (10 W/mK) than AISI1055 (53 W/mK). Heat becomes more difficult to conduct away from heat source for material with low thermal conductivity.

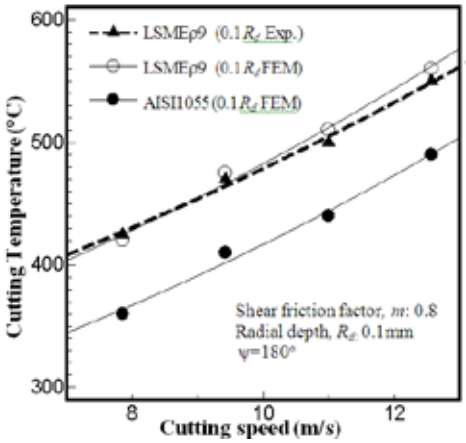

Fig. 10 Effect of cutting speed on cutting temperature

This phenomenon can be explained in Figure 11 where steady state analyses for temperature distributions inside the workpiece when machining both materials at 754m/min was done.

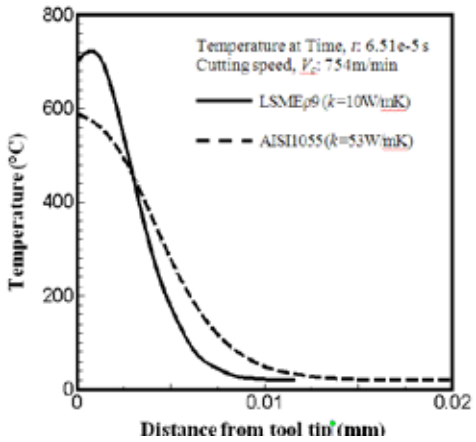

Fig. 11 Temperature distribution comparison for different thermal conductivity

Workpiece temperature near the tool tip for LSMEρ9 is higher than AISI1055. Nevertheless, cutting temperature decreases drastically for LSMEρ9 workpiece along the cross sectional compared to AISI1055 workpiece. This is due to the quantity of heat travels inside LSMEρ9 workpiece is lower than AISI1055 in single unit time.

C. Different Tool Diameter Analysis

Figure 12 shows the comparison between estimated cutting tool temperatures with the experimental approach for machining LSMEρ9 using less than 2mm ball end mill.

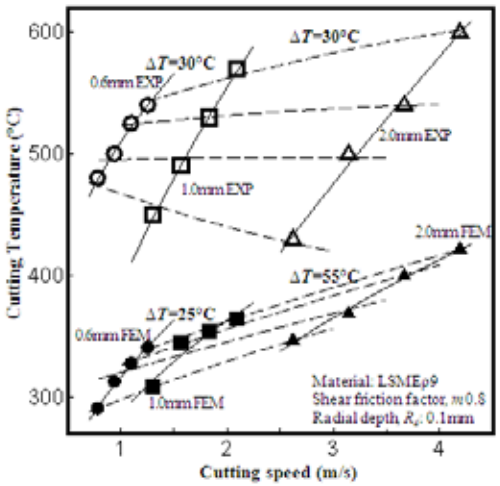

Fig. 12 Comparison between estimated cutting temperatures with the experiment

According to Figure 12, the estimated cutting temperature shown large errors when compare with experimental approach. This is due to the simulation were under the ideal cutting process where other parameters such as tool wear are neglected. This error could be explained in Figure 13 and Figure 14.

Figure 13 shows the relationship between cutting force and Merchant shear angle evolution with increasing cutting speed when machining LSMEρ9 for different cutting tool diameter.

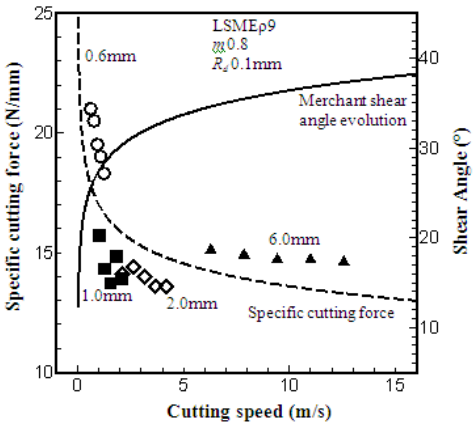

Fig. 13 Effect of cutting speed on specific cutting force and Merchant shear angle evolution

From Figure 13, increasing cutting speed tend to decrease specific cutting force. The Merchant shear angle evolution is obtained from G. Sutter *et al.* [23] is shown in Eq. 6.

$$\theta_M = (0.5\pi - 0.704 V^{-0.248} + \alpha)/2 \quad (6)$$

Where θ_M is the Merchant shear angle, V is the cutting speed and α is the rake angle.

Specific cutting force slightly decreases at high cutting speed. This phenomenon can be explained using Merchant shear angle evolution where shear angle drastically increase at lower cutting speed but slightly increase at high cutting speed. It is well-known that shear angle have a direct effect on cutting force [24].

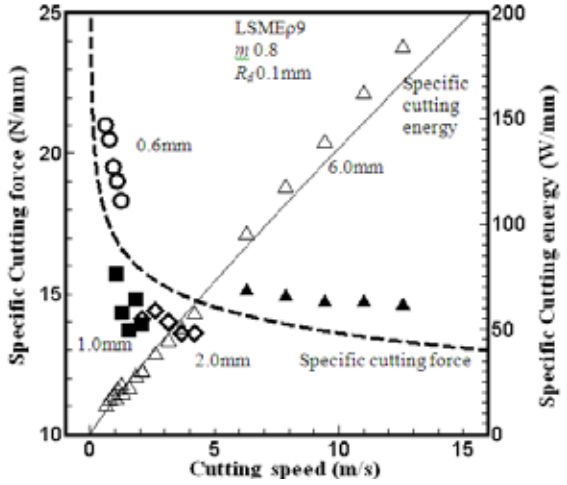

Fig. 14 Effect of cutting speed on cutting force and cutting energy

Figure 14 shows the relationship between cutting force and cutting energy with increasing cutting speed in ideal cutting (simulation). Although the cutting forces is high at low cutting speed, the cutting energy is low compare to cutting energy at high cutting speed according to Eq. 3. This analysis could explain the cutting force evolution and cutting energy at high cutting speed since it is impossible to obtain cutting forces during experiment due to measurement tool limitation [6].

According to G. Newby *et al.*, end milling operation that less than 1.6mm diameter are consider as micro end milling operation where the cutting tool suffer aggressive feed per tooth per radius compare to conventional milling operations [25]. This process could increase tool wear rate such as adhesive, chatter or flank wear for end mill less than 1.6mm and could be related to increasing cutting temperature during the experiment. Furthermore, LSMEρ9 have high material hardness that could contribute tool wear rate and temperature increases.

Study on small ball end mill cutting performance with diameter less than 2.0mm is important to produce high precision mould. Further investigation need to be done to explain this phenomenon such as effect of tool wear on cutting temperature using finite element analysis.

IV. Conclusion And Recommendation

i. In this study, FE analyses of cutting force and cutting temperature on the machining process by cemented carbide tool on laser sintered material (LSMeρ9) and mild steel (AISI1055) workpiece were done.

ii. The analyses were executed using 2 dimensional orthogonal cutting with thermo-mechanical plane strain model.

iii. The machinability of laser sintered material (LSMeρ9) was analyzed by mean of cutting force and cutting temperature generated during the machining process by FEM.

iv. Shear friction factors range between 0.6-0.9 are used in the study and the results are compared with the experimental results in terms of maximum cutting force and cutting temperature.

v. From the study, 2D shear friction model, m0.8 estimated cutting force with lowest errors (10%). Shear friction coefficient could be different when apply 3D FEM model.

vi. The study shows that the cutting force increases with the increases in shear friction factor and radial depth of cut (R_d) due to increasing frictional stress and chip removal rate (mm^3/s).

vii. Cutting edge temperature increases with increasing cutting speed due to increasing cutting energy. Estimated cutting temperature for AISI1055 and LSMEρ9 shows below 5% errors when comparing with experimental results.

viii. AISI 1055 shows higher cutting force than laser-sintered materials, LSMEρ9 due its higher Young modulus. However, LSMEρ9 developed higher cutting edge temperature than AISI 1055 due to its lower thermal conductivity.

ix. Lower thermal conductivity material conduct less heat in single unit time thus it is known that temperature in LSMEρ9 decreases drastically when measurement distance farther away from the tool tip.

x. Laser sintered material; LSMep9 can be considered having low machinability compared to mild steel due to higher cutting temperature near to the tool tips. Plus with its high hardness, this phenomenon could increase tool wear and roughness to the machined surface.

xi. Decreasing tool diameter will increase specific cutting force (N/mm) and decreasing specific cutting energy (W/mm) due to decreasing cutting speed. FEM simulation results show decreasing cutting temperature when cutting tool diameter decreases.

xii. When comparing cutting tool temperature for less than 2mm diameter ball end mill, estimated cutting temperature shows large error compared to experimental approach.

xiii. This shown that the ball end milling process in the experimental approach was not an ideal cut where other parameters such as cutting tool life and tool wear must be investigate to gain extra knowledge in machining laser sintered materials LSMEρ9 with high precision.

xiv. This paper emphasized the application of 2D orthogonal model in simulating high speed machining. For further future investigation, 3D FEM simulation could be applied in obtaining more precise results and data.

Acknowledgement

Author would like to show greatest appreciation to Universiti Malaysia Pahang (UMP) and Ministry of High Education (KPT) for funding the master study.

References

[1] R. C. Dewes and D. K. Aspinwall, "A review of ultra high speed milling of hardened steels," *Journal of Materials Processing Technology,* Vol. 69, No. 1-3, pp. 1-17, 1997.

[2] D. King and T. Tansy, "Rapid tooling Selective laser sintering injection tooling," *Journal of Materials Processing Technology,* Vol. 132, No. 1-3, pp. 42, 2003.

[3] S. Ramada and P. Dickens, "Rapid tooling analysis of Stereolithography injection mould tooling," *International Journal of Machine Tools and Manufacture,* Vol. 47, No. 5, pp. 740-747, 2007.

[4] S. Kalpakjian and S. R. Schmidt, "Manufacturing engineering and technology," 4th ed., pp. 1148, Prentice Hall International, 2000.

[5] B. U. Guzzle and I. Lazuli, "An enhanced force model for sculptured surface machining," *Machining Science and Technology,* Vol. 8, No. 3, pp. 431, 2004.

[6] A. Yassin, "Experimental Study on Machinability of Laser-sintered Material in Ball end Milling," Phd Thesis, Kanazawa University, 2009.

[7] L. Filice, F. Micari, S. Rizzuti and D. Umbrello, "Dependence Of Machining Simulation effectiveness On Material And Friction Modelling," *Machining Science and Technology,* Vol. 12, No. 3, pp. 370.

[8] T. Ozel, "The Influence of Friction Models On Finite Element Simulations of Machining," *Int. Journal of Tools and Manufacturing,* Vol. 46, pp. 518-530 , 2006.

[9] E. Usui and Shirakashi, "Mechanics of Machining from Descriptive to Predictive Theory," *On the Art of Cutting Metals* - 75 Years Later, No. 7, pp.13-55.

[10] J. S. Strenkowski and J. T. Carroll, "A Finite Element Model of Orthogonal Metal Cutting," *Trans. ASME J. Eng. Ind.,* Vol. 107, pp. 349, 1985.

[11] J. P. Davim and C. Maranhao, "A Study of Plastic Strain and Plastic Strain Rate in Machining of Steel AISI 1045 Using FEM Analysis," *Materials and Design,* Vol. 30, pp. 160-165, 2009.

[12] J. P. Davim, C. Maranhao, M. J. Jackson, G. Cabral and J. Gracio, "FEM analysis in high speed machining of aluminium alloy (Al7075-0) using polycrystalline diamond (PCD) and cemented carbide (K10) cutting tools," *Int. Journal, Advanced Manufacturing Technology,* Vol. 39, pp. 1093, 2008.

[13] D. Umbrello, "Finite element simulations of conventional and high speed machining of Ti6Al4V alloy," *Journal of Materials Processing Technology,* Vol. 196, No. 1-3, pp. 79-87, 2008.

[14] T. Ozel and T. Altan, "Process simulation using finite element method - prediction of cutting forces, tool stresses and temperature in high speed flat end milling," *Int. Journal of Machine Tools & Manufacturing,* Vol. 40 pp. 713-718, 2000.

[15] T. Furumoto, T. Ueda, M. S. Abdul Aziz, A. Hosokawa and R. Tanaka, "Study on reduction of residual stress induced during rapid tooling process – influence of heating conditions on residual stress," *Key Engineering Materials,* pp. 447-448, 785-789.

[16] A. Yassin, T. Ueda, T, Furumoto, A. Hosokawa, R. Tanakaq and S. Abe, "Experimental investigation on cutting mechanism of laser sintered material using small ball end mill," *Journal of Materials Processing Technology,* Vol. 209, pp. 5680, 2009.

[17] B. M. Ergatoudis, O. C. Irons and Zienkiewics, "Curved, isoparametic 'Quadrilateral' element for finite element analysis," *Int. J. Solids Structures,* Vol. 4, pp. 31-42, 1968.

[18] S. Kato, K. Yamaguchi, M. Yamada, "Stress distribution at the interface between tool and chip in machining," *Trans ASME J Eng., Ind .,* Vol. 94, pp. 683–689, 1972.

[19] N. A. Abukhshim, P. T. Mativenga, M. A. Sheikh, "Heat generation and temperature predicition in metal cutting: review and implications for high speed machining," *Int. Journal of Machine Tools & Manufacture,* Vol. 46, pp. 782-800, 2006.

[20] R. T. Coelho, E. G. Ng , M. A. Elbestawi, "Tool wear when turning hardened AISI 4340 with coated PCBN tools using finishing cutting conditions," *Int. Journal of Mahcine Tools and Manufacture,* Vol. 472, No. 2, pp. 63-272 , 2007.

[21] N. A. Abukhshim, P.T. Mativenga and M. A. Sheikh, "Investigation of heat partition in high speed turning of high strength alloy steel," Int. *Journal of Machine Tools & Manufacture,* Vol. 45, pp. 1687, 2005.

[22] A. Hosokawa, Z. P. Zhou, K. Yamada and T. Ueda, "Studies on High-speed Milling with Small Ball End Mill: Temperature Distribution on Flank Face of Cutting Tool," *Journal of Japanese Society Precision Engineering,* Vol. 70, No. 12, pp. 1527-1532.

[23] G. Sutter, "Chip geometries during high-speed machining for orthogonal cutting conditions," *International Journal of Machine Tools & Manufacture,* Vol. 45, pp. 719-726, 2005.

[24] E. Trent, P. Wright, " Metal Cutting," Fourth Edition, Butterworth Heinemann, US, 2000.

[25] G. Newby, S. Venkatachalan, S.Y. Liang, "Empirical analysis of cutting force constants in micro-end-milling operations," *Journal of Materials Processing Technology,* pp. 192-193, 41-47, 2007.